Research Article

Chuji Zheng, Jun Wang*, Hengjuan Liu, Hota GangaRao, and Ruifeng Liang

Characteristics and microstructures of the GFRP waste powder/GGBS-based geopolymer paste and concrete

https://doi.org/10.1515/rams-2022-0005
received September 25, 2021; accepted November 19, 2021

Abstract: A novel method is developed for reusing the waste glass fiber-reinforced polymer (GFRP) powder as a precursor in geopolymer production. Several activation parameters that affect the workability and strength gain of GFRP powder-based geopolymers are investigated. The results of an experimental study reveal that the early strength of GFRP powder-based geopolymer pastes develops slowly at ambient temperature. The highest compressive strength of GFRP powder-based geopolymer pastes is 7.13 MPa at an age of 28 days. The ratio of compressive strength to flexural strength of GFRP powder-based-geopolymers is lower than that of fly ash and ground granulated blast furnace slag (GGBS)-based geopolymers, indicating that the incorporation of GFRP powder can improve the geopolymer brittleness. GGBS is incorporated into geopolymer blends to accelerate the early activity of GFRP powder. The binary geopolymer pastes exhibit shorter setting times and higher mechanical strength values than those of single GFRP powder geopolymer pastes. The GGBS geopolymer concrete mixture with 30 wt% GFRP powder displayed the highest compressive strength and flexural strength values and was less brittle. The developed binary GFRP powder/GGBS-based geopolymers reduce the disadvantages of single GFRP powder or GGBS geopolymers, and thus, offer high potential as a building construction material.

Keywords: waste glass fiber reinforced powder, geopolymer, mechanical property

1 Introduction

Glass-fiber-reinforced polymers (GFRPs) form the largest segment of the composite industry, offer the advantages of excellent designability, lightweight, high specific strength and stiffness, and good corrosion resistance, and are mainly used in aerospace engineering, automotive industry, power generation, and infrastructure design [1–3]. Increasing GFRP applications has raised serious concerns in the composite industry regarding the waste management of GFRP materials. The resins used as the matrix of GFRPs can be divided into thermosetting or thermoplastic resins. It is more difficult to recycle thermosetting GFRPs than thermoplastic GFRPs because irreversible reactions occur during their manufacture and permanent cross-links form in their molecular chains [4]. The techniques for recycling thermosetting GFRP wastes are categorized as mechanical, thermal, and chemical methods [5], but all suffer from certain limitations including high energy consumption, high cost, long cycle time, and the release of toxic gases [6,7]. This study provides new insights and information on the potential use of waste GFRP powder as a precursor in the production of geopolymer pastes and concretes. The workability and mechanical and microstructural characteristics of GFRP powder-based geopolymers are investigated to understand the mechanism of the alkali-activated GFRP powder. A geopolymer combination of GFRP powder and ground granulated blast-furnace slag (GGBS) is designed to compensate for the lack of aluminum in GFRP powder. The binary geopolymers show excellent workability and mechanical properties compared with geopolymers with only GGBS or GFRP powder alone. The resulting GFRP powder/GGBS-based geopolymers can be used as construction materials, which are expected to remarkably reduce CO_2 emissions and energy consumption over cementitious materials, and thus, resolve

* **Corresponding author: Jun Wang,** Bridge Engineering Department, College of Civil Engineering, Nanjing Tech University, Nanjing 211816, China, e-mail: wangjun3312@njtech.edu.cn
Chuji Zheng: Bridge Engineering Department, College of Civil Engineering, Nanjing Tech University, Nanjing 211816, China
Hengjuan Liu: Nanjing Urban Construction Tunnel and Bridge Wisdom Management Co., Ltd, Nanjing 211816, China
Hota GangaRao, Ruifeng Liang: Department of Civil and Environmental Engineering, West Virginia University, Morgantown, WV 26506, USA

the environmental issues associated with GFRP waste disposal. The process of this study is shown in graphical abstract.

Geopolymers are produced from chemically activated silica and alumina-rich raw materials using an alkaline solution, which results in an amorphous three-dimensional matrix of tetrahedrally linked aluminosilicates [8]. The geopolymerization process is an efficient method for converting aluminosilicate waste materials into useful binders. Most industrial by-products are rich in SiO_2 and Al_2O_3 with potential gelling or pozzolanic activity to produce alkali-activated materials [9]. Geopolymer concrete exhibits comparable or better mechanical properties than conventional cement concrete and is considered to be a new generation of eco-friendly building material [10]. Fly ash (FA) and GGBS are the most common precursors used to produce geopolymers [11–13]. Although FA-based geopolymers have excellent engineering properties, their early strength usually develops slowly at ambient temperature, which severely limits their extensive application in engineering. The addition of GGBS is beneficial to improve the early strength and shorten the setting time of geopolymers However, the incorporation of a certain extent of GGBS yields a deleterious effect on shrinkage [14]. The optimization and combination of different types of industrial solid wastes as precursors to produce geopolymer may therefore have a synergistic effect on the engineering properties.

The main chemical constituents of GFRP waste powder are silica, calcium, and alumina, along with magnesium and iron oxides. During the geopolymerization reaction, silica, calcium, and alumina in GFRP powder are expected to react with an alkaline solution to form sodium-aluminosilicate-hydrate or calcium-aluminosilicate-hydrate gels. Farinha et al. [15] investigated the influence of GFRP waste as a fine aggregate in cement-based mortar and revealed that the mortar with 50% of GFRP waste as natural aggregate substitution had the best physicomechanical properties. Although alkaline-activated GFRP powder has not yet been reported in the literature, considerable effort has been devoted to develop alkali-activated waste glass cement for use as a construction material because the waste glass can supply reactive silica [16,17]. Waste glass powder (WGP) can be applied as a partial GGBS replacement to prolong the setting time of GGBS geopolymers due to the lower alkali reactivity of WGP. The incorporation of WGP also reduces the drying shrinkage and alkali-silica reaction expansion of GGBS geopolymers [18]. Burciaga-Diaz et al. [19] and Shoaei et al. [20] reported that the incorporation of 30% WGP yields an optimal compressive strength of metakaolin and GGBS-based geopolymers. Tho-in et al. [21] found an optimum WGP content of 20% in FA-based geopolymers, whereas further increasing the WGP replacement levels yields a lower alumina/silica ratio, leading to the formation of an inferior aluminosilicate product. Rashidian-Dezfouli and Rangaraju [22] demonstrated that ground glass fiber (GGF) can be effectively activated by an alkali activator to produce geopolymer pastes. Their study showed that GGF and FA-based geopolymers perform considerably better than GP-based geopolymers in sodium sulfate solution because stable aluminosilicate gel forms in the former [23].

The amount of resin in GFRP used for structural applications ranges from 25 to 55% [24]. Hence, the influence of resin in GFRP waste powder-based geopolymers cannot be neglected. The thermosetting resin commonly used in GFRP includes epoxy, vinyl ester resin, and polyester resin. Tabatabaeian et al. [25] investigated the performance of pervious concrete incorporated by polyester and epoxy resin. Their results revealed that the addition of polyester or epoxy resin can significantly increase the mechanical and durability properties of pervious concrete and that the incorporation of polymer resin yields better compressive performance than that involving epoxy resin. This is because the silane coupling agent in polyester creates strong bonding between the resin and microfillers [25]. Saludung et al. [26] reported that the inclusion of 1% epoxy resin remarkably reduced the alkali leaching rate during the early immersion period (5 days) because the epoxy resin reacts with the geopolymer matrix due to the formation of OH groups. Moreover, increasing the epoxy resin content enhances the flexural strength to compressive strength ratio for ambient curing geopolymers, which suggests that epoxy resin improves the geopolymer brittleness [26]. Zhang [27] stated the metakaolin-based geopolymers incorporated with epoxy resin require a longer curing time to reach complete internal condensation stabilization. The highest compressive strength of the geopolymer was achieved for a resin content of 10%, whereas excessive resin hindered the polycondensation reaction [27].

The purpose of this work is to investigate the potential use of GFRP waste powder as a precursor in the production of geopolymers. Several activation parameters that affect the workability and strength gain of GFRP powder-based geopolymers and binary GFRP powder/GGBS-based geopolymers are investigated. The workability and mechanical properties of binary GFRP powder/GGBS-based geopolymer concrete are explored, in which the effects of the GFRP powder content, water to binder ratio (W/B), aggregate to binder ratio (A/B), and sand to aggregate ratio (S/A) are taken into account. X-ray diffraction (XRD), Fourier transform infrared (FTIR) spectroscopy, and scanning electron microscopy (SEM) coupled with

energy-dispersive X-ray spectroscopy (EDS) are applied to investigate the microstructural characteristics of the GFRP powder-based geopolymers and binary GFRP powder/GGBS-based geopolymers.

2 Materials and experimental program

2.1 Materials

The GFRP waste powder was provided by Nanjing Spare Composites Co., Ltd, China, in which the volume percent of the E glass fiber and unsaturated polyester resin were 72 and 28%, respectively. The GFRP powder had a particle size between 1.583 and 37.841 μm with a mean particle size (D_{50}) of 13.506 μm. The bulk density of the GFRP powder was 525.5 kg·m^{-3}. The particle size of the GGBS ranged between 2.102 and 40.532 μm with D_{50} = 15.937 μm. The GGBS bulk density was 1,320 kg·m^{-3}. XRD analyses indicated that the main crystalline phases of the GFRP powder were calcite and portlandite, and those of the GGBS were identified as quartz, calcite, and calcium silicate (Figure 1). The chemical compositions of the GFRP powder and GGBS were determined by X-ray fluorescence spectroscopy, and the results are given in Table 1.

The alkaline solution was prepared as a combination of sodium silicate (Na_2SiO_3) and 19.5 M sodium hydroxide (NaOH). The modulus ratio (SiO_2/Na_2O) of sodium silicate was 3.2, where Na_2O = 8.54% and SiO_2 = 27.3%. Sodium hydroxide was prepared by dissolving NaOH pellets (98% purity) in water.

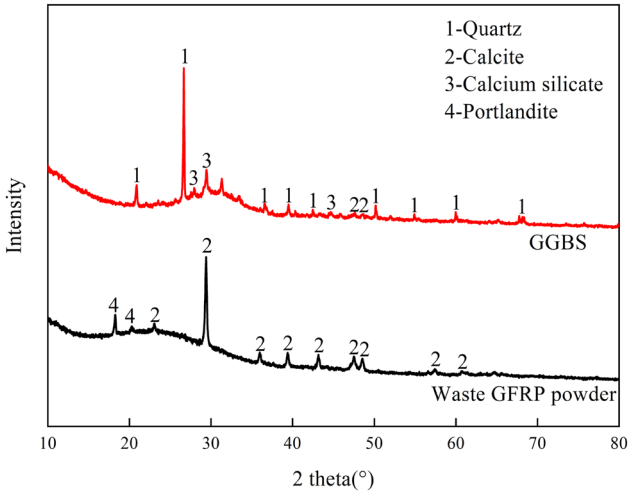

Figure 1: XRD pattern of the GFRP waste powder and GGBS.

Natural river sands with a fineness modulus of 2.7 and a specific density of 2.65 g·cm^{-3} were used as the fine aggregates. Crushed limestone aggregates with a diameter of 15–30 mm and a specific density of 2.67 g·cm^{-3} were used as the coarse aggregates.

Polycarboxylate superplasticizer was used as the water-reducing admixture in the geopolymer concrete.

2.2 Preparation of geopolymers

The mixture proportion of the geopolymer paste was determined based on the orthogonal experimental design method. For single GFRP powder-based geopolymers, the orthogonal testing parameters included the activator concentration, liquid to solid (L/S) ratio, and activator solution modulus. The Taguchi orthogonal arrays and mixtures for the full factorial experiments of the single GFRP powder-based geopolymers are listed in Table 2. For the binary GFRP powder/GGBS-based geopolymers, the GFRP waste powder was added as a GGBS replacement in weight percentages of 30, 50, and 70%, and the effects of GFRP powder content, activator concentration (75, 80, 85%), L/S (0.7,0.8, 0.9), and activator solution modulus (1.3, 1.4, 1.5) were considered in the mixture design (Table 3).

2.3 Preparation of the geopolymer concrete

The effects of the GFRP powder content, sand to aggregate ratio (S/A = 0.25, 0.30, 0.35), aggregate to binder ratio (A/B = 4.0, 4.5, 5.0), and water to binder ratio (W/B = 0.45, 0.5, 0.55)

Table 1: Chemical compositions of the GFRP powder, FA, and GGBS

Chemical composition (wt%)	GFRP powder	GGBS
SiO_2	33.71	34.66
Al_2O_3	10.62	17.78
CaO	20.57	34.15
MgO	3.45	6.04
Fe_2O_3	0.63	1.03
SO_3	0.98	1.65
K_2O	0.32	0.27
Na_2O	0.21	0.39
TiO_2	0.51	0.66
LOI	28.12	0.84

Note: Loss of ignition (LOI) is calculated through weight after firing of materials.

Table 2: Orthogonal array and the mixture of GFRP powder-based geopolymers

Trial	Factor A	Factor B	Factor C	GFRP powder ($kg \cdot m^{-3}$)	NaOH ($kg \cdot m^{-3}$)	Na_2SiO_3 ($kg \cdot m^{-3}$)	H_2O ($kg \cdot m^{-3}$)
G1	0.7	75	1.3	1,472	107.7	665.1	257.6
G2	0.7	80	1.4	1,472	102.5	721.8	206.1
G3	0.7	85	1.5	1,472	97.7	778.1	154.6
G4	0.8	75	1.4	1,472	109.8	773.4	294.4
G5	0.8	80	1.5	1,472	105.1	837.0	235.5
G6	0.8	85	1.3	1,472	139.5	861.4	176.6
G7	0.9	75	1.5	1,472	110.9	882.7	331.2
G8	0.9	80	1.3	1,472	147.8	912.1	265.0
G9	0.9	85	1.4	1,472	140.0	986.1	198.7

Note: Factor A is L/S ratio, factor B is the activator concentration (%), and factor C is the modulus of the activator solution.

were taken into account in the geopolymer concrete mixture design, as shown in Table 4. A geopolymer concrete specimen without GFRP powder was also prepared as a reference. The activator concentration, L/S, and activator solution modulus were determined based on the test results of the binary geopolymer paste. For each geopolymer concrete mixture, the content of the polycarboxylate superplasticizer was 2% of the total mass of the GFRP powder and GGBS.

After casting, the geopolymer concrete specimens and molds were covered with a plastic film to prevent moisture loss and cured at room temperature for 24 h. The specimens were then demolded and cured in a standard curing room at 20 ± 2°C and relative humidity of 95% until reaching the desired curing age (3, 7, 28 days).

2.4 Experimental program

2.4.1 Workability

The properties of the geopolymer mixtures in the fresh state were characterized by the setting time and flowability. The setting time of the fresh pastes was determined in accordance with Chinese Standard GB/T 1346-2011 [28]. The flowability of the fresh pastes was determined in accordance with the Chinese Standard GB/T 8077-2012 [29]. The setting time and flowability of the fresh geopolymer concrete were determined in accordance with the Chinese Standard GB/T 50080-2016 [30]. Both the reported setting time and flowability value were taken as the average of three measurements obtained at room temperature. Three duplicate coupons were tested for each material composition for workability tests.

2.4.2 Mechanical tests

The properties of the geopolymer pastes in the hardened state were characterized by their compressive and flexural strengths. The flexural strength of prismatic hardened paste samples with dimensions of 40 mm × 40 mm × 160 mm at 3, 7, and 28 days was tested in accordance with the Chinese Standard GB/T 17671-1999 [31]. At least three replicate samples for each mix were measured for every age to obtain an average value. Compressive strength tests were conducted on two broken pieces of the prismatic specimens after the flexural strength test. The compressive loading rate was 2.4 $kN \cdot s^{-1}$ and the loading area was 40 mm × 40 mm.

The compressive strength, elasticity modulus, and flexural strength of the geopolymer concrete were determined in accordance with the Chinese Standard GB/T50081-2019 [32]. Three replicate cubic specimens (150 mm × 150 mm × 150 mm) were prepared for testing the compressive strength of each mixture at 3, 7, and 28 days. The elasticity modulus of three replicate prismatic samples (150 mm × 150 mm × 300 mm) from each mixture was tested at every age. Strain gauges (length = 10 mm) were bonded to the surfaces of the prismatic samples to record the stress–strain relationship during compression. The samples for flexural testing were prismatic with dimensions of 100 mm × 100 mm × 400 mm. Three duplicate coupons were tested for each material composition for mechanical tests.

2.4.3 Microstructure analysis

XRD (Ultima IV, Japan) analysis was performed to identify the mineral phases of the GFRP powder-based geopolymers and binary GFRP powder/GGBS-based geopolymers at 3, 7, and 28 days. FTIR (Nicolet iS50, USA)

Table 3: Mixture of GFRP powder/GGBS-based geopolymers

Mixture	GFRP ($kg·m^{-3}$)	GGBS ($kg·m^{-3}$)	Modulus of the activator solution	Activator concentration (%)	L/S	Na_2SiO_3 ($kg·m^{-3}$)	NaOH ($kg·m^{-3}$)	Water ($kg·m^{-3}$)
GS-0-1.5-80-0.7	/	1,472	1.5	80	0.7	732.7	91.8	205.9
GS-30-1.5-80-0.7	441.6	1030.4	1.5	80	0.7	732.7	91.8	205.9
GS-50-1.5-80-0.7	736.0	736.0	1.5	80	0.7	732.7	91.8	205.9
GS-70-1.5-80-0.7	1030.4	441.6	1.5	80	0.7	732.7	91.8	205.9
GS-30-1.3-80-0.7	441.6	1030.4	1.3	80	0.7	710.6	114.8	205.0
GS-30-1.4-80-0.7	441.6	1030.4	1.4	80	0.7	721.8	102.5	206.1
GS-30-1.5-75-0.7	441.6	1030.4	1.5	75	0.7	686.9	86.0	257.4
GS-30-1.5-85-0.7	441.6	1030.4	1.5	85	0.7	780.6	97.8	154.5
GS-30-1.5-80-0.8	441.6	1030.4	1.5	80	0.8	836.9	104.9	235.8
GS-30-1.5-80-0.9	441.6	1030.4	1.5	80	0.9	941.6	117.9	265.3

spectroscopy was used to measure the structural properties of the geopolymers over a wavenumber range of 400–4,000 cm^{-1}. Changes in the geopolymer microstructures at different curing ages were examined by SEM (Sigma300, ZEISS, Germany) coupled with EDS.

3 Results and discussion

3.1 GFRP powder-based geopolymer paste

3.1.1 Setting time

The test results of the GFRP powder-based geopolymer pastes are listed in Table 5. The initial setting time of the fresh pastes was in the range of 138–720 min, and the final setting time was in the range of 450–1,560 min. Both the initial and final setting times of the GFRP powder-based geopolymer pastes were longer than those of the high-calcium FA geopolymer pastes containing 18.45 wt% CaO, for which the initial and final setting times were 105 and 185 min, respectively [33]. However, the final setting times of the most of GFRP-based geopolymers were considerably shorter than that of the low-calcium FA geopolymer containing 2.5 wt% CaO, for which the final setting time was >1,260 min [34]. According to the Chinese Standard GB/T 175-2007 [35], the initial setting time of ordinary Portland cement (OPC) pastes should be no less than 45 min, and the final setting time should be no more than 600 min. The setting time of the GFRP powder geopolymer pastes with L/S of 0.8, activator concentration of 85% and activator solution modulus of 1.3 meets the requirements of the Chinese Standard GB/T 175-2007.

The setting time primarily depends on the formation of the C–S–H or C–A–S–H gel products [36]. High CaO contents tend to accelerate the hydration reaction of geopolymer pastes [37]. The setting time is also related to the mass ratio of SiO_2 to Al_2O_3 and their total contents. Although the CaO content of the GFRP powder is higher than that of high-calcium FA geopolymer in ref. [33], the mass ratio of SiO_2 to Al_2O_3 in the former (3.17) is considerably higher than that of the latter in ref. [33] (1.55). The total SiO_2 and Al_2O_3 contents in the GFRP powder are also lower than that of the FA in ref. [33]. Higher SiO_2 to Al_2O_3 mass ratios or lower aluminosilicate content prolong the geopolymer setting time. The unsaturated polyester resin in GFRP powder may also retard the hydration reaction of alkali-activated glass fiber powder. An adjustment of the SiO_2 to Al_2O_3 ratio in raw materials is therefore an

Table 4: Mixture constituents of GFRP powder/GGBS-based geopolymer concrete

Mixture	W/B	S/A	A/B	GFRP powder ($kg \cdot m^{-3}$)	GGBS ($kg \cdot m^{-3}$)	Fine aggregate ($kg \cdot m^{-3}$)	Coarse aggregate ($kg \cdot m^{-3}$)	Na_2SiO_3 ($kg \cdot m^{-3}$)	NaOH ($kg \cdot m^{-3}$)	Water ($kg \cdot m^{-3}$)
GC-1	0.5	0.35	5	0	361.8	632	1,175	194.3	24.3	54.5
GC-2	0.5	0.35	5	180.9	180.9	632	1,175	194.3	24.3	54.5
GC-3	0.5	0.35	5	253.3	108.6	632	1,175	194.3	24.3	54.5
GC-4	0.45	0.35	5	109.8	256.2	640	1,188	176.6	22.1	49.6
GC-5	0.5	0.35	5	108.6	253.3	632	1,175	194.3	24.3	54.5
GC-6	0.55	0.35	5	104.1	242.7	605.8	1,162	211.4	26.5	59.3
GC-7	0.5	0.25	5	108.5	253.1	453	1,356	193.9	24.3	54.5
GC-8	0.5	0.30	5	108.6	253.4	541.8	1,266	194.3	24.3	54.5
GC-9	0.5	0.35	4	127.5	297.4	594.5	1,105	228.1	28.6	64.1
GC-10	0.5	0.35	4.5	117.1	273.3	615	1,143	209.6	26.3	58.9

effective strategy to control the setting time of GFRP powder-based geopolymers.

The relationship between setting time and the three mixture factors is shown in Figure 2. The response index for each factor is the average of the three values for the trial mixtures containing the particular factor. The influence of factor A (L/S) on the setting time is notably greater than those of factors B (activator concentration) and C (activator solution modulus). Increasing the L/S from 0.7 to 0.8 had an insignificant effect on the initial and final setting times; however, further increasing the L/S led to a dramatic increase of the setting time. This may be attributed to the increased water content that is associated with the higher alkaline solution content. Both the initial and final setting times decreased with an increasing activator concentration. This may be because higher activator concentrations improve the dissolution rate of the GFRP powder, thus enhancing the geopolymerization process. The investigated range of activator solution modulus (1.3–1.5) had an insignificant effect on the initial and final setting times.

3.1.2 Flowability

The relationship between the flow value and three mixture factors is shown in Figure 3. The flowability of the GFRP powder geopolymer pastes was in the range of 214–290 mm. The effect of factor A (L/S) on the flowability was more significant than that of the other factors. The flow value increased with increasing L/S and decreased with increasing activator concentration. This is because higher L/S or lower activator concentration values can slow down the chemical reaction of the GFRP powder with the activator solution, thus enhancing the flowability. An increase of the activator solution modulus from 1.3 to 1.4 led to an increase in the flow value, whereas a further increase to 1.5 led to a slight decrease of the flow value.

Table 5: Test results of trial mixes of the GFRP powder-based geopolymer paste

Mix	Initial setting time (min)/δ (%)	Final setting time (min)/δ (%)	Flowability (mm)/δ (%)	Compressive strength (MPa)/δ (%)			Flexural strength (MPa)/δ (%)		
				3 day	7 day	28 day	3 day	7 day	28 day
G1	180/3.6	720/3.1	230/3.6	0	2.29/0.2	4.36/0.3	0	0	1.62/0.1
G2	198/3.2	708/3.6	240/2.6		2.65/0.3	6.01/0.2			1.97/0.3
G3	192/2.1	660/5.0	245/4.4		2.79/0.1	5.34/0.2			1.71/0.1
G4	360/3.5	960/2.6	285/3.2		1.62/0.1	4.07/0.4			1.28/0.2
G5	210/4.6	720/4.7	247/4.6		1.50/0.1	3.47/0.2			0.97/0.1
G6	138/2.6	450/1.5	214/3.0		1.65/0.1	7.13/0.2			2.06/0.3
G7	720/4.6	1440/4.4	287/3.8		1.02/0.1	2.49/0.3			0.93/0.2
G8	540/3.6	1560/4.4	290/4.6		0.71/0.2	1.94/0.4			1.41/0.1
G9	360/4.4	1320/3.6	272/5.3		0.94/0.1	3.19/0.3			1.48/0.3

Note: δ is the coefficient of variation.

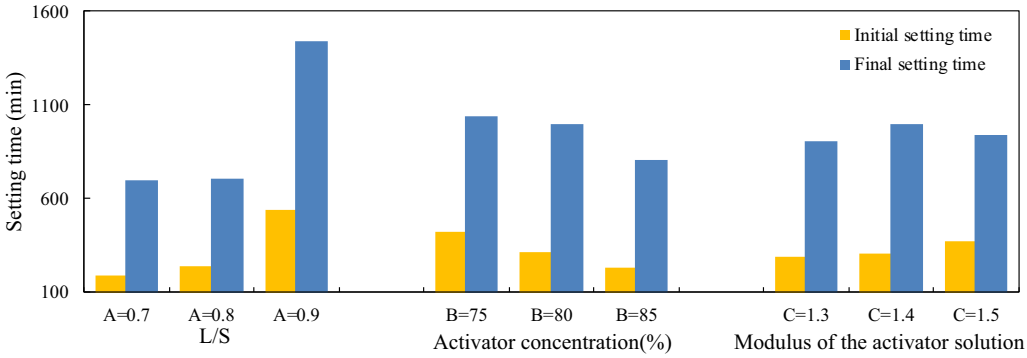

Figure 2: Relationship between the setting time of GFRP powder geopolymer pastes and three mix factors.

3.1.3 Compressive strength

The relationship between compressive strength and the three mixture factors is shown in Figure 4. The 3-day compressive strength and 3- and 7-day flexural strengths were undetectable owing to the poor early reactivity of the GFRP powder. The 7- and 28-day compressive strengths varied from 0.71 to 2.79 MPa and 1.94 to 7.13 MPa, respectively, for the GFRP powder-based geopolymer paste with different mixture factors. The compressive strength of the GFRP powder-based geopolymer paste increased with curing age. This is because the reactivity of the GFRP powder was gradually stimulated over time, thus improving the development of the geopolymer compressive strength later. The strength development of geopolymers is related to the particle size, active components, early reactivity, and SiO_2 to Al_2O_3 ratio of the raw materials [33]. Increasing the particle size of the raw materials can slow the

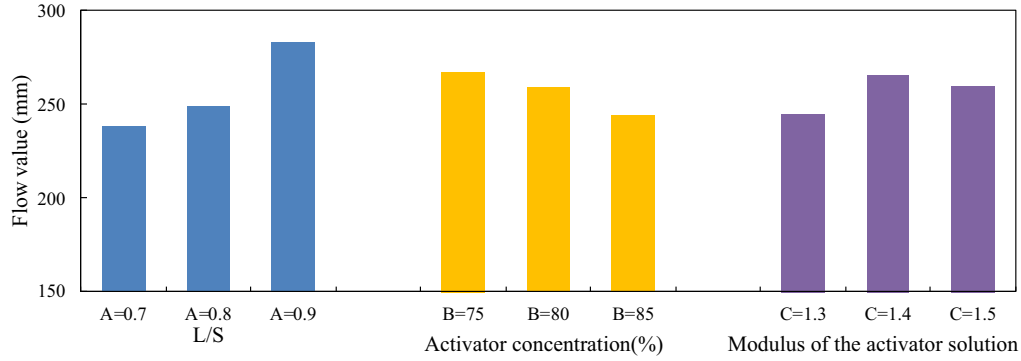

Figure 3: Relationship between the flow value of GFRP powder geopolymer pastes and three mix factors.

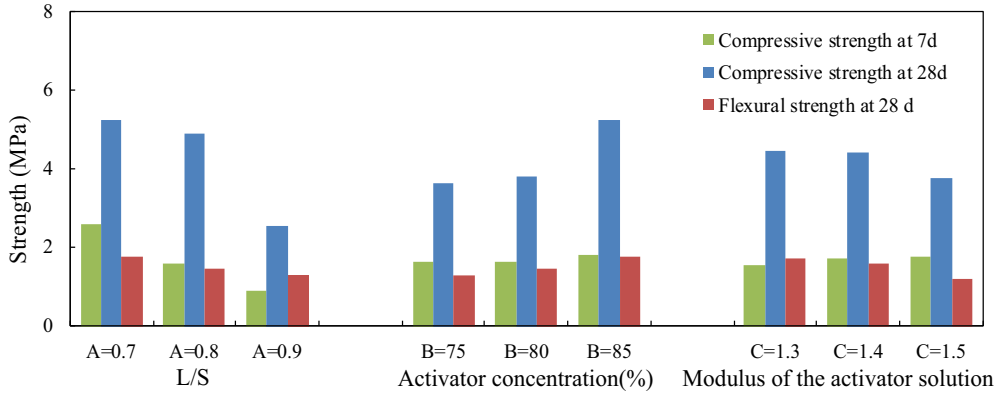

Figure 4: Relationship between the strength of GFRP powder geopolymer pastes and three mix factors.

dissolution rate, and eventually, have a negative effect on the compressive strength development of geopolymers [38]. The low Al_2O_3 content exerts a strong negative effect on the strength development and chemical reaction rate of C–A–S–H gel products [39]. In this study, the poor early reactivity, large particle size (larger than FA in ref. [33]), and low Al_2O_3 content (lower than FA and GGBS) of the GFRP powder retarded the geopolymerization process, thus leading to slow development of the compressive strength.

The 7- and 28-day compressive strengths of the GFRP powder-based geopolymer pastes both decreased with increasing L/S ratio. This may be because the higher water content owing to the increased solution content negatively affected the compressive strength [34]. The alkali concentration had an insignificant effect on the 7-day compressive of the geopolymer pastes, but increasing the alkali concentration led to an increase in the 28-day compressive strength. Increasing the alkali concentration improved the dissolution rate of the GFRP powder, thus improving the geopolymerization process. The activator solution modulus had an insignificant effect on the 7-day compressive of the geopolymer pastes, while increasing the activator solution modulus from 1.4 to 1.5 led to a decrease of the 28-day compressive strength. This is because higher activator solution moduli contain low NaOH contents, and a reduction of the NaOH molarity slows the dissolution rate of the aluminosilicate materials [34].

3.1.4 Flexural strength

The variation trends of the 28-day flexural strength with the three mixture factors are similar to those of the 28-day compressive strength, as shown in Figure 4. The ratios of the compressive strength to flexural strength (RCF) of the GFRP powder-based geopolymers at 28 days were in the range of 1.38–3.58. The RCF is an important indicator that reflects geopolymer brittleness. Higher RCF values indicate that the material is more brittle. The RCF values of the FA-steel slag (SS)–GGBS geopolymers were in the range of 5.98–7.45 [36], which are higher than those of the GFRP powder geopolymer, and thus, indicates that the resin in the GFRP powder can improve the geopolymer brittleness.

3.1.5 Microstructural properties

The XRD results of a typical GFRP powder-based geopolymer mixture (specimen G6) at ages of 3, 7, and 28 days are presented in Figure 5. The crystalline phases of the

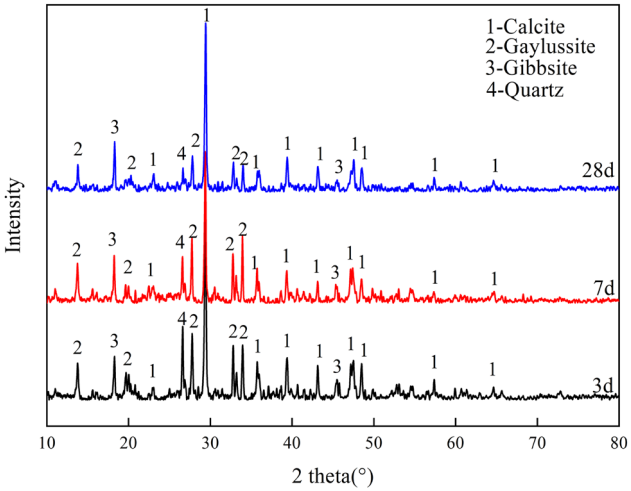

Figure 5: XRD analysis of geopolymer pastes containing only the GFRP powder (G6).

hardened pastes at different curing ages mainly included calcite ($CaCO_3$), gaylussite ($Na_2Ca(CO_3)_2(H_2O)_5$), gibbsite ($Al(OH)_3$), and quartz (SiO_2). The existing calcite and quartz were derived from the unreacted GFRP powder. The quartz peak intensity decreased with increasing curing ages. This decrease suggested that the reactivity of the GFRP powder increased gradually during geopolymerization, resulting in the consumption of the quartz phase [40]. Gaylussite was identified as one of the main crystalline phases [41]. The formation of gaylussite indicates that for early ages, a preferential reaction occurred between the atmospheric CO_2 and Ca^{2+} released from the partial dissolution of the GFRP powder. This phase is unstable and transforms to $CaCO_3$ and hydrotalcite, followed by the precipitation of the C–A–S–H gel [41]. The gaylussite peak intensity thus decreased with increasing curing ages. The presence of gibbsite minerals indicated that there was $Al(OH)_3$ present that had not yet reacted.

The FTIR spectra of a typical GFRP powder-based geopolymer mixture (specimen G6) at ages of 3, 7, and 28 days are shown in Figure 6. The band observed around 3,337 cm^{-1} is related to the bending vibration of O–H, and the bands that appear around 1,650 cm^{-1} are assigned to the stretching vibration of O–H [42]. The increase of intensities with curing ages can be explained by an improved alkaline attack and dissolution of the GFRP powder by the OH^- groups. The absorption band that appears around 1,403 cm^{-1} is attributed to the vibration of O–C–O bonds due to carbonization. The bands from 984 to 1,010 cm^{-1} are assigned to the asymmetric stretching vibrations of Si–O–T (where T represents Si or Al), which can be ascribed to the development of the amorphous N–A–S–H gel and a C–S–H gel network [43]. With increasing

curing time, this peak shifted to lower wavenumbers thus indicating that the formed gels were more stable. The peaks around 875 cm^{-1} are assigned to O–C–O stretching and vibration bands due to carbonization. Additionally, the band around 444 cm^{-1} is assigned to the flexural vibrations of the Si–O–Si bonds.

The SEM images of specimen G6 at ages of 3, 7, and 28 days after compression are presented in Figure 7. The microstructure of specimen G6 at an age of 3 days is composed of flocculent gels and cracks. The EDS results of the flocculent network gel products of this specimen indicate that O, Si, Ca, and C are the principal elements in the gel products, and Na and Mg are the minor elements. The precursors contain a considerable amount of SiO_2 and CaO, and thus, Si and Ca ions were released during the geopolymerization to form C–S–H gel products. The Al/Si, Na/Si, and Ca/Si atomic ratios for the gel products of this specimen at an age of 3 days were 0.272, 0.076, and 0.339, respectively, indicating that most of the gel products are either C–S–H gel or C–A–S–H gel. The C ions were released from the unsaturated polyester resin in the GFRP waste powder due to the –COOH, $–CH_3$, and –CH groups in the resin matrix.

The microstructure of specimen G6 at an age of 7 days exhibited layered gels, voids, and cracks, and the Al/Si, Na/Si, and Ca/Si atomic ratios of the layered gels determined by EDS were 0.137, 0.675, and 0.516, respectively. The presence of a considerable amount of Na in the gel products can be attributed to the formulation of N–A–S–H [33]. At an age of 28 days, cluster gels and cracks are observed in specimen G6, and the Al/Si, Na/Si, and Ca/Si ratios for the cluster gels of this specimen were 0.143, 0.714, and 0.086, respectively. The Ca/Si ratio at an age of 28 days was considerably lower than those at early ages, which verifies the increased dissolution of Ca ions and subsequent formation of either C–S–H gel or C–A–S–H gel. An Al/Si ratio in the range of 0.2–0.4 is suitable for the mechanical strength development of geopolymers [44]. The low Al/Si ratio is related to the low Al_2O_3 content in the GFRP powder geopolymer.

3.2 GFRP powder/GGBS-based geopolymer pastes

3.2.1 Setting time

The test results of the GFRP powder/GGBS-based geopolymer pastes are listed in Table 6. The initial and final setting times of the fresh pastes were in the range of 120–175 and 155–263 min, respectively, both of which are shorter than those of the geopolymer pastes with GFRP powder alone. When the GFRP powder content was increased from 0 to 70%, the initial setting time increased from 120 to 160 min, and the final setting time increased from 155 to 215 min. An exceedingly short setting time may limit the application of GGBS in engineering projects. Increasing the GFRP powder content tends to retard the geopolymerization process of GGBS-based geopolymers owing to the increased SiO_2 to Al_2O_3 mass ratio and SiO_2 and Al_2O_3 contents in the raw materials. The early activity of the GFRP powder-based geopolymer can therefore be accelerated by the incorporation of GGBS.

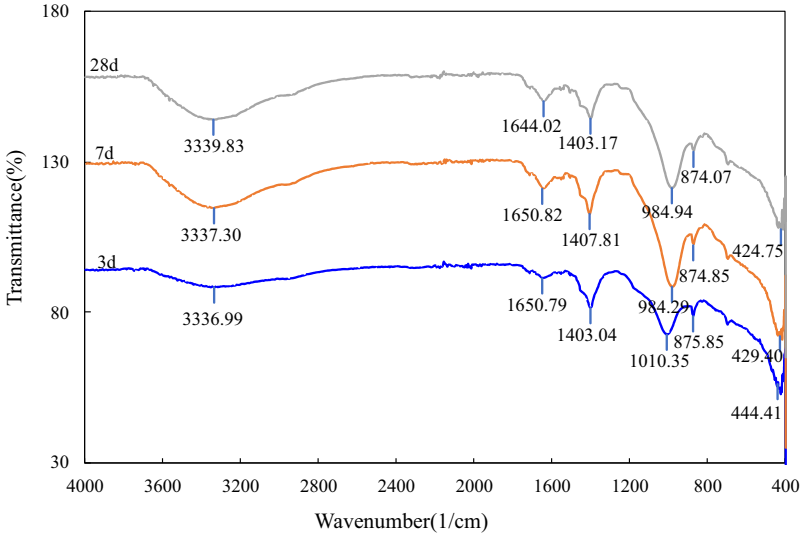

Figure 6: FTIR spectra of geopolymer pastes containing only the GFRP powder (G6).

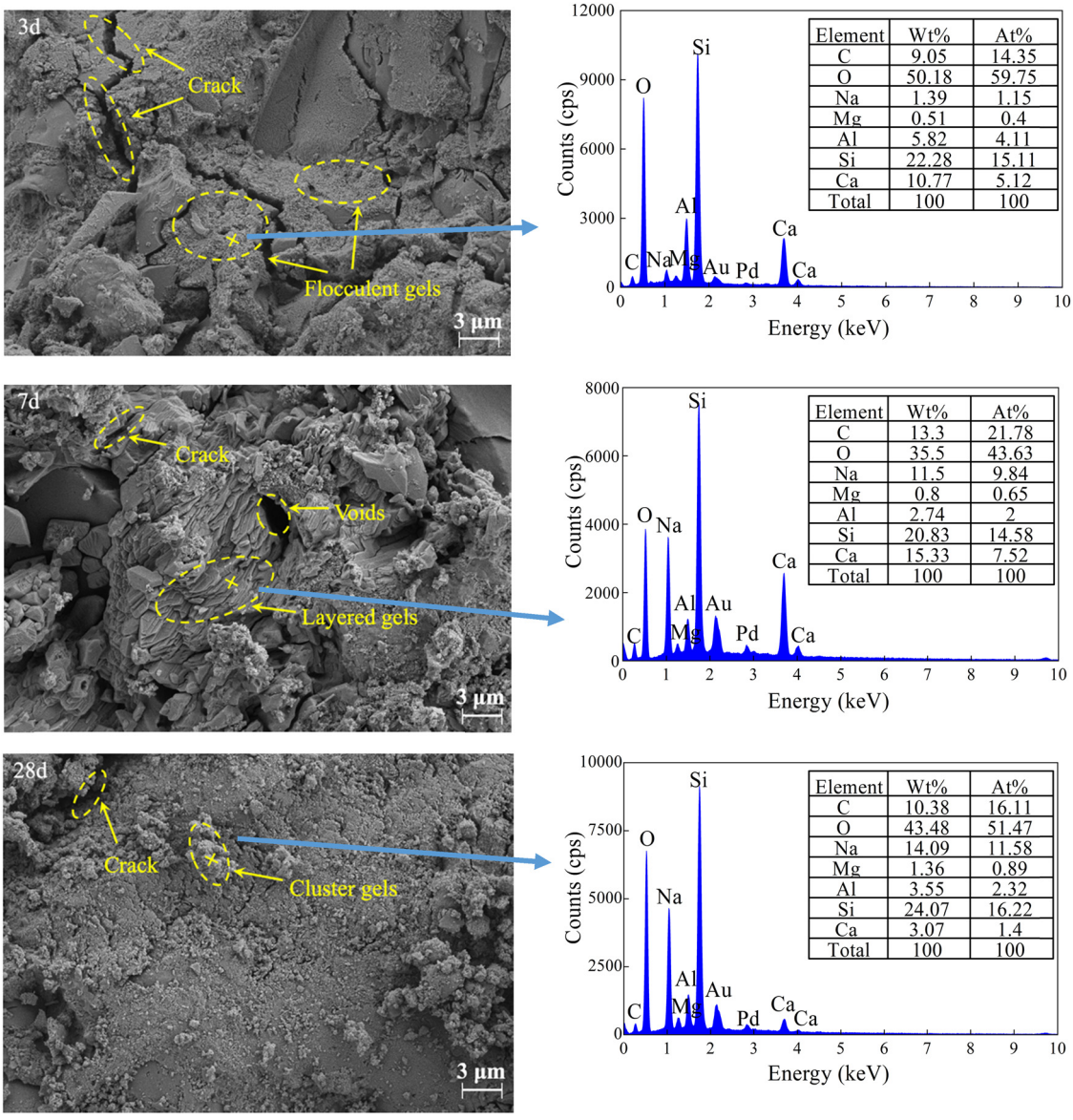

Figure 7: SEM images and EDS analysis of specimen G6 at different ages.

As shown in Figure 8, an increase of the L/S value from 0.7 to 0.9 led to a gradual increase of the setting time, whereas an increase of the activator concentration from 75 to 85% led to a gradual decrease of the setting time. These trends agree with those of the geopolymers with GFRP alone. An increase of the activator solution modulus from 1.3 to 1.4 had an insignificant effect on the initial and final setting times, whereas further increasing the activator solution modulus led to a significant increase of the setting time. This may be because the reduced NaOH molarity slows the dissolution rate of the aluminosilicate precursors.

3.2.2 Flowability

The relationship between the flow value of the GFRP powder/GGBS geopolymer pastes and four mixture factors is shown in Figure 9. The flow value gradually increased with increasing GFRP powder content. This is because excessive resin may hinder the geopolymerization process of the glass fiber powder. Increasing the L/S or decreasing the activator concentration tended to increase the flow value, which is in agreement with the trends of the geopolymers with GFRP alone. Increasing the activator solution modulus led to a gradual reduction of the flow

Table 6: Test results of GFRP powder/GGBS-based geopolymers pastes

Mixture	Initial setting time (min)/δ (%)	Final setting time (min)/δ (%)	Flowability (mm)/δ (%)	Compressive strength (MPa)/δ (%)			Flexural strength (MPa)/δ (%)		
				3 day	7 day	28 day	3 day	7 day	28 day
GS-0-1.5-80-0.7	120/2.6	155/4.4	191/2.6	29.3/2.5	36.1/3.7	40.5/2.7	2.3/1.0	3.8/1.4	5.4/1.8
GS-30-1.5-80-0.7	148/2.0	200/3.1	202/3.0	33.9/2.3	40.3/2.3	43.1/1.9	5.7/0.8	6.6/0.7	7.1/0.4
GS-50-1.5-80-0.7	157/3.1	214/4.6	231/4.2	24.8/2.1	27.9/3.4	30.1/4.0	4.4/0.7	5.1/1.7	6.2/0.5
GS-70-1.5-80-0.7	160/3.6	215/4.2	248/2.6	15.1/3.9	19.9/2.6	25.8/3.4	3.9/2.2	4.5/1.0	4.9/2.3
GS-30-1.3-80-0.7	129/2.1	155/3.5	216/2.5	21.7/2.3	27.8/2.6	29.5/4.3	2.9/1.5	5.2/1.3	5.7/1.2
GS-30-1.4-80-0.7	132/3.5	161/4.0	210/2.3	26.8/3.0	29.9/3.7	31.2/2.6	4.2/1.3	5.6/1.8	5.9/0.8
GS-30-1.5-75-0.7	150/4.4	209/2.5	208/2.5	23.7/3.1	29.1/1.4	32.2/4.3	2.7/1.6	4.2/0.4	6.0/0.6
GS-30-1.5-85-0.7	142/1.5	184/3.1	166/2.1	20.5/1.6	26.8/4.2	29.2/2.9	2.2/0.6	4.0/2.4	5.1/1.2
GS-30-1.5-80-0.8	168/3.2	248/2.6	215/1.5	24.5/2.1	28.9/3.4	30.5/3.3	3.2/0.7	3.6/1.3	4.2/0.8
GS-30-1.5-80-0.9	175/5.0	263/2.1	224/5.2	22.9/2.9	27.8/4.0	28.5/1.3	2.1/0.8	2.6/0.3	3.8/0.1

Note: δ is the coefficient of variation.

values. Higher activator solution moduli were associated with lower NaOH contents. At lower NaOH solution molarity, more calcium ions are available to react with water to form C–S–H and C–A–H gels, thus the flowability decreases [34].

3.2.3 Compressive strength

Figure 10a shows the compressive strength of the GFRP powder/GGBS geopolymer pastes as a function of the GFRP powder content. The compressive strength of the GFRP powder/GGBS geopolymer pastes was remarkably enhanced compared with that of the geopolymer pastes with GFRP powder alone. The 3-day compressive strengths of the geopolymers were approximately 60–85% of their 28-day compressive strength. The high 3-day compressive strength is attributed to the positive effect of GGBS on the early strength development (Table 6). The compressive strength of geopolymers containing 30 wt% GFRP powder was higher than those of the geopolymers with GGBS alone. The high early reactivity of GGBS in alkali solution makes it highly susceptible to shrinkage and microcrack development, which increases the porosity and leads to strength loss [45]. The incorporation of a certain content of the GFRP powder can slow down the reactive rate of GGBS in an alkali solution. Wang et al. [46] reported that the addition of a proper dosage of epoxy (<4 wt%) into a geopolymer can fill in the gaps and reduce the number of harmful pores and the pore diameter. When the GFRP powder content exceeded 30 wt%, the compressive strength of the GFRP powder/GGBS geopolymer pastes gradually decreased with increasing GFRP powder content. This may be attributed to the high dosage of resin-impregnated on the surface of the glass fiber powder, which hinders the further dissolution of Si and Al. The incorporation of an optimal amount of GFRP powder into GGBS geopolymers can therefore effectively minimize the disadvantages of both the GFRP powder and GGBS precursors.

As shown in Figure 10b, the early and 28-day compressive strengths of the GFRP powder/GGBS geopolymer pastes decreased by ~33% when the L/S was increased from 0.7 to 0.9. Figure 10c indicates that the maximum compressive strength of the GFRP powder/GGBS geopolymer pastes was obtained at an activator concentration of 80%. Above this level, the compressive strength decreased with increasing activator concentration. This is because the excess alkali leads to the increasing dissolution of silica and other constituents. The excess silica ions in the solution react with carbon dioxide and form sodium carbonate crystals that destabilize the microstructure, thus reducing the

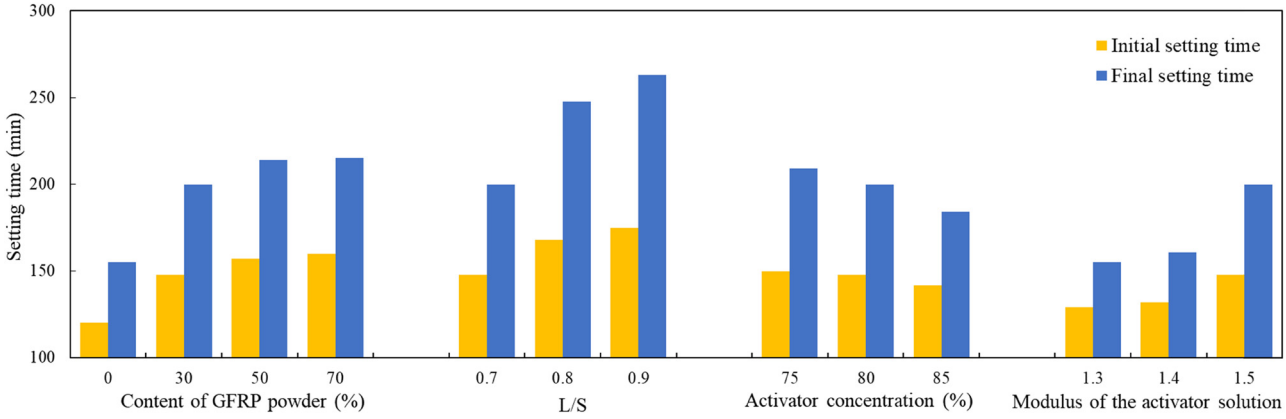

Figure 8: Relationship between the setting time of GFRP powder/GGBS geopolymer pastes and the four mix factors.

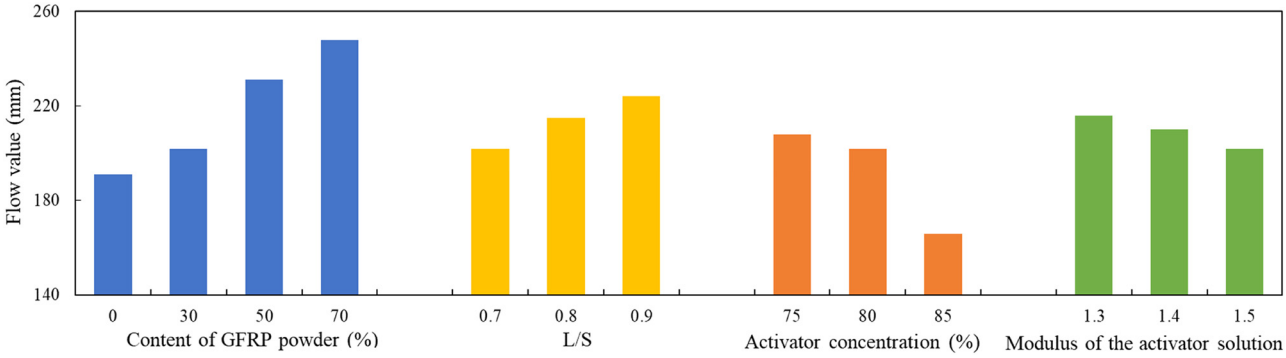

Figure 9: Relationship between the flow value of GFRP powder/GGBS geopolymer pastes and the four mix factors.

mechanical strength [47]. When the activator solution modulus was increased from 1.3 to 1.5, the early and 28-day compressive strengths of the GFRP powder/GGBS geopolymer pastes increased by ~35%, as shown in Figure 10d.

3.2.4 Flexural strength

The effects of the four mixture factors on the flexural strength of the GFRP powder/GGBS geopolymer pastes are shown in Figure 11. The variation trends of the flexural strength with the four mixture factors are similar to those of the compressive strength. The geopolymer paste containing 30 wt% GFRP powder exhibited the highest flexural strength. Reducing the L/S value or increasing the activator solution modulus led to an increase of the flexural strength. The flexural strength of the GFRP powder/GGBS geopolymer pastes with an activator concentration of 80% was higher than those of the geopolymer pastes with activator concentrations of 75 and 85%.

The relationship between the RCF of the GFRP powder/GGBS geopolymer pastes and the four mixture factors is shown in Figure 12. The RCF values of the geopolymers at all ages are in the range of 3.87–10.9. Most of the RCF values decreased with the curing age. This is because the reactivity of the GFRP powder was gradually stimulated and the formed gel products filled in the gaps of the matrix, thus improving the brittleness of the GFRP powder/GGBS-based geopolymers. At ages of 3, 7, and 28 days, the RCF values of the geopolymers containing 30 wt% GFRP powder were, respectively, 53, 36, and 19% lower than those of the geopolymers with GGBS alone. The GFRP powder with a low early activity present in the matrix may act as microaggregates to inhibit shrinkage and prevent crack development, thereby improving the brittleness of the material [36]. Further increasing the GFRP powder content led to an insignificant change in the RCF values. The RCF increased with increasing L/S. This may be because excessive water caused larger shrinkage during the drying process than required. At an age of 3 days, the RCF value of the geopolymer pastes with an activator concentration of 80% was lower than those of the geopolymer pastes with activator concentrations of 75% and 85%, whereas the activator concentration had an insignificant influence on the 28-day RCF. The

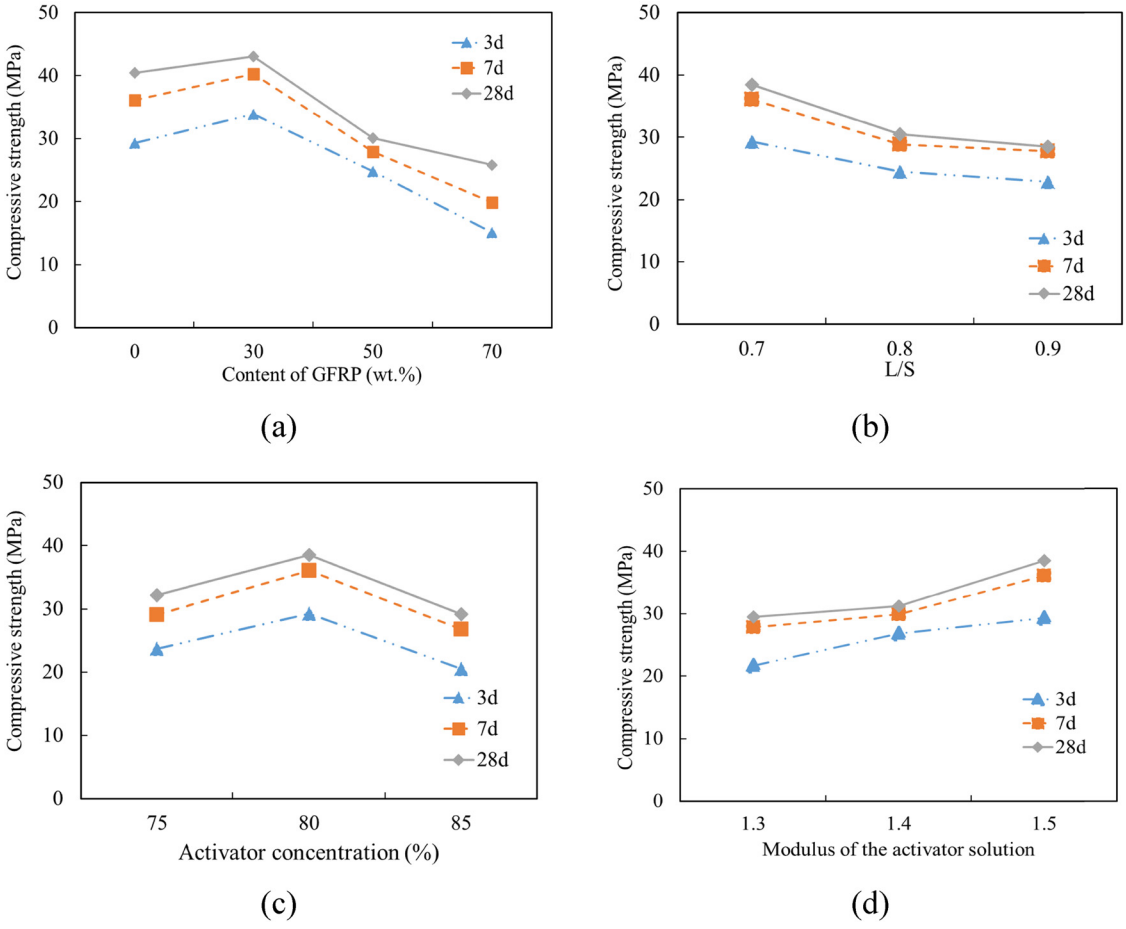

Figure 10: Compressive strength of GFRP powder/GGBS based geopolymer pastes: (a) influence of the content of GFRP, (b) influence of L/S, (c) influence of the activator concentration, and (d) modulus of the activator solution.

activator solution modulus had an insignificant effect on the RCF for all ages.

3.2.5 Microstructural properties

The XRD results of the hardened GFRP powder/GGBS geopolymer pastes with the highest 28-day compressive strength (specimen GC-5) are presented in Figure 13 at different ages. The crystalline phases of the hardened pastes at different curing ages were mainly calcite ($CaCO_3$), quartz (SiO_2), and calcium silicate hydrate. The existing calcite and quartz were derived from unreacted raw materials. The calcium silicate hydrate confirms the presence of a C–S–H phase. The calcium silicate hydrate peak intensities remained nearly unchanged for different curing times, which indicates that this compound is a residue of the anhydrous GGBS [48].

The FTIR spectra of specimen GC-5 at different ages are shown in Figure 14. The bands observed around 3,351 and 1,641 cm^{-1} are related to the bending and stretching vibrations of O–H, respectively. However, the OH^- groups are indiscernible in the 3-day specimen. This is because the high reactivity of GGBS in the alkali activators consumed substantial amounts of water at an early age. Under steam curing conditions, the OH^- groups continuously permeated in the mixture and they were then observed in the specimens with ages of 7 and 28 days. The absorption band of the O–C–O carbonate groups at 1,417 cm^{-1}, asymmetric stretching vibrations of Si–O–T around 1,000 cm^{-1}, O–C–O stretching and vibration bands at 874 cm^{-1}, and flexural vibrations of Si–O–Si bonds from 464 to 440 cm^{-1} were observed in specimen GC-5, which is consistent with those of the geopolymer with GFRP powder alone.

The SEM images of specimen GC-5 at different ages after compression are presented in Figure 15. A considerable amount of cluster gels are observed on this specimen at all ages. The EDS results reveal that O, Ca, C, Si, and Al are the principal elements in the gel products. The precursors contain a considerable amount of SiO_2, CaO, and

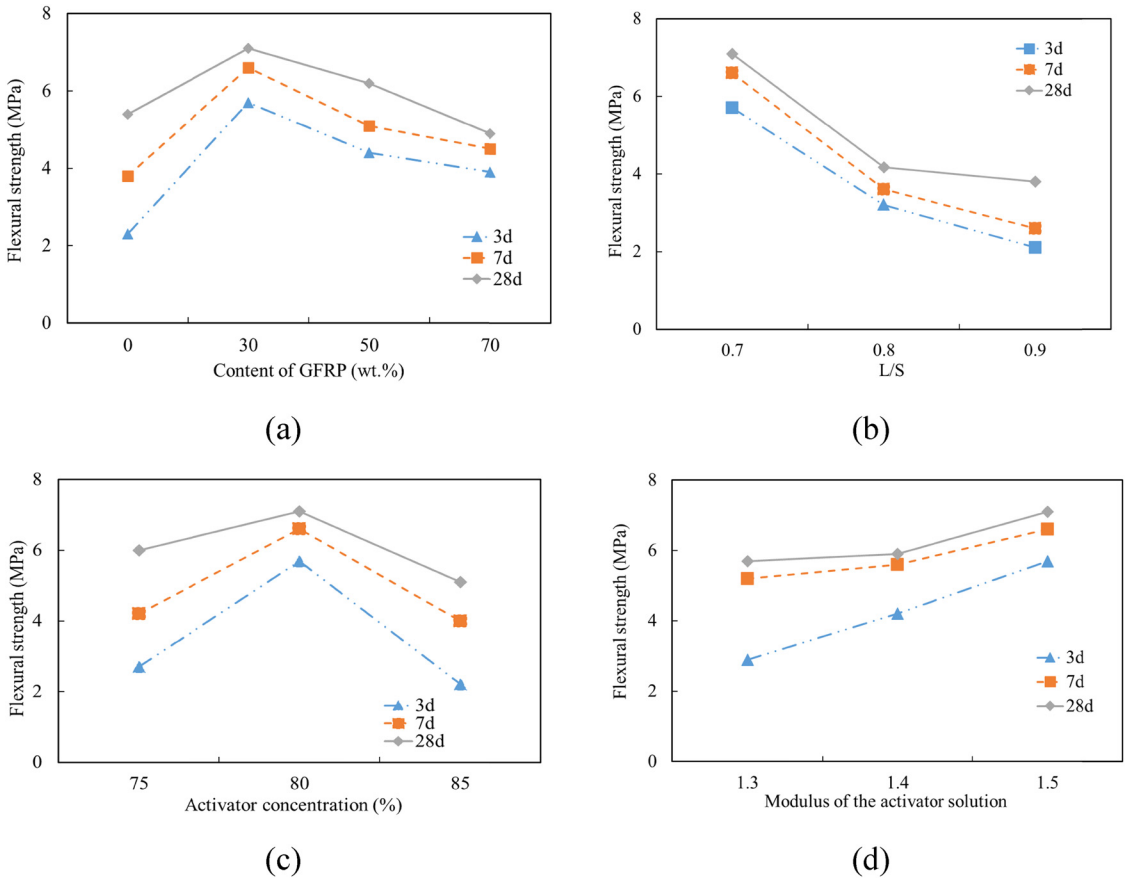

Figure 11: Flexural strength of GFRP powder/GGBS based geopolymer pastes: (a) influence of the content of GFRP, (b) influence of L/S, (c) influence of the activator concentration, and (d) modulus of the activator solution.

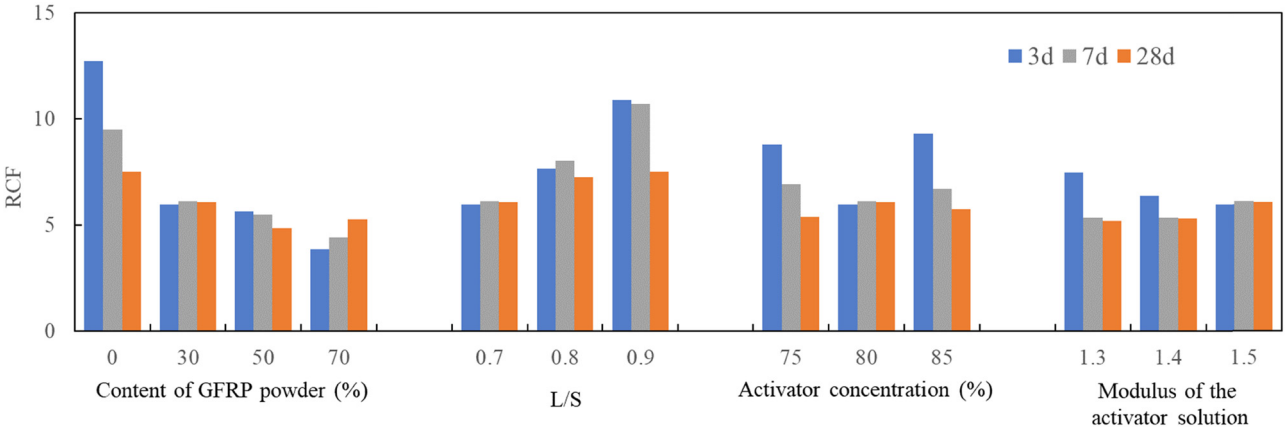

Figure 12: Relationship between RCF of GFRP powder/GGBS geopolymer pastes and four mix factors.

Al_2O_3, thus Si, Ca, and Al ions were released during geopolymerization to form C–S–H or C–A–S–H gel products. The Al/Si, Na/Si and Ca/Si atomic ratios for the gel products at an age of 3 days were 0.36, 0.27, and 1.93, respectively. The Ca contents and Ca/Si ratio of the GFRP powder/GGBS geopolymer paste were higher than those of the geopolymer pastes with GFRP powder alone owing to the higher CaO content in GGBS. The Al/Si, Na/Si, and Ca/Si atomic ratios for the gel products at 7 days were 0.35, 0.33, and 0.81, respectively. The Ca/Si ratio remarkably decreased with increasing curing age from 3 to 7 days due to the increased dissolution of Ca ions. The

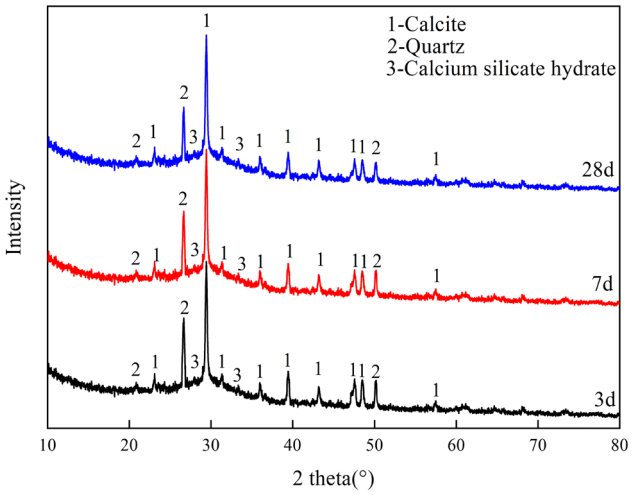

Figure 13: XRD analysis of GFRP powder/GGBS geopolymer pastes (GC-5).

Al/Si, Na/Si, and Ca/Si atomic ratios of the gel products at 28 days varied insignificantly compared with those of the gel products at 7 days, which suggests a nearly complete geopolymerization at 7 days. The Al/Si atomic ratio was in the range of 0.24–0.36 at ages of 3, 7, and 28 days, which is suitable for mechanical strength development.

3.3 GFRP powder/GGBS-based geopolymer concrete

3.3.1 Setting time

The test results of the GFRP powder/GGBS geopolymer concrete are listed in Table 7. The initial and final setting times were in the range of 164–220 and 189–265 min, respectively. Figure 16 shows the relationship between the setting time of the GFRP powder/GGBS geopolymer concretes and the four mixture factors. For identical W/B, S/A, and A/B ratios, the setting time increased with increasing GFRP powder content. Increasing W/B from 0.45 to 0.55 led to a prolonged setting time. This is because the mixing of water interferes with the dissolution of the raw materials and subsequent polycondensation [49]. When A/B was increased from 4 to 5, the setting time was decreased. The lower A/B values represent not only more binder material but also a more free liquid solution of the geopolymer concrete mixture. Higher amounts of free liquid solution lubricate the geopolymer concrete mixture and prolong the setting time [50]. The setting time decreased with increasing S/A. This is because the larger amount of aggregates provided a larger specific surface area, which was covered by more moisture.

3.3.2 Slump

The relationship between the slump of the GFRP powder/GGBS geopolymer concretes and the four mixture factors is shown in Figure 17. All of the GFRP powder/GGBS geopolymer concrete mixtures achieved a slump value of >160 mm, which implies that the GFRP powder/GGBS geopolymer concretes can be regarded as high-flow concretes according to the Chinese standard GB50164-2011 [51]. In general, higher GFRP powder contents resulted in higher slump values of the geopolymer concrete mixture. This is because the reactive rate of the GFRP powder in the alkaline solution is slower than that of the GGBS.

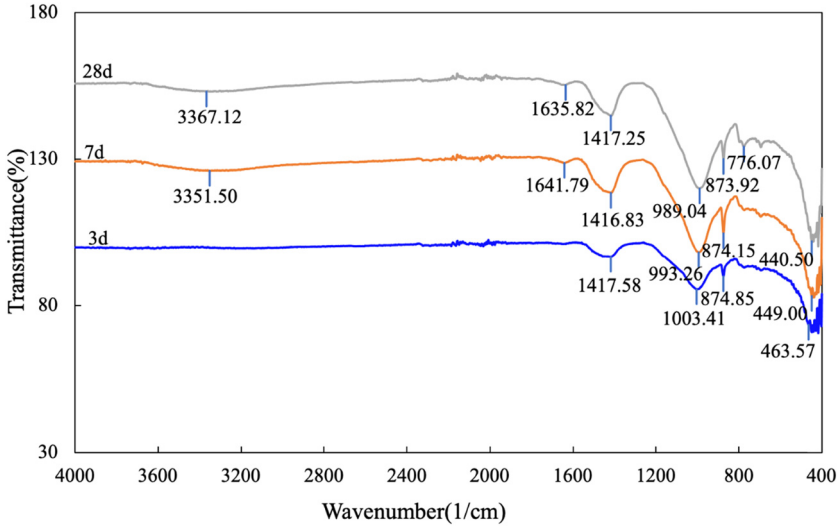

Figure 14: FTIR spectra of GFRP powder/GGBS geopolymer pastes (GC-5).

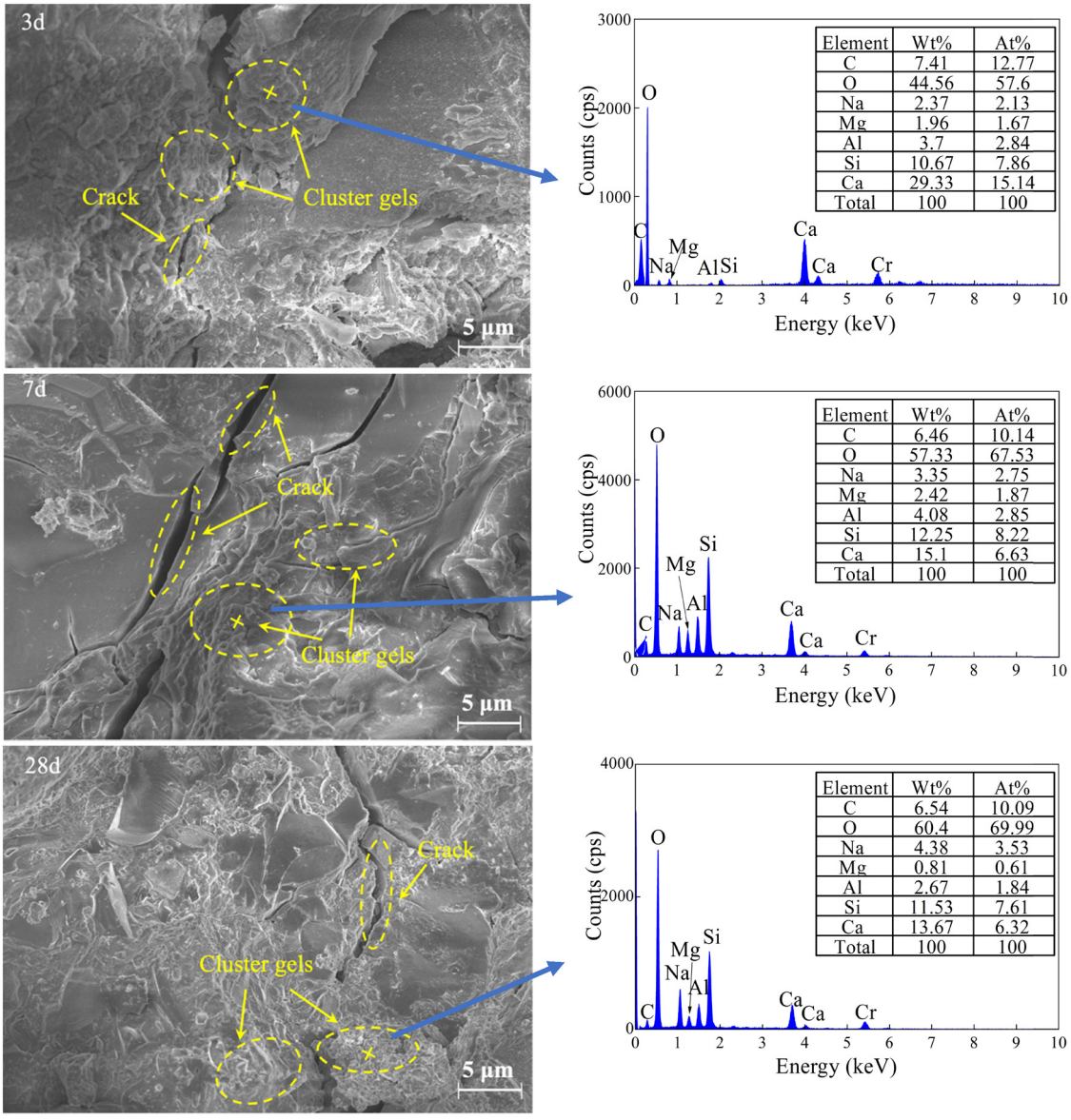

Figure 15: SEM images and EDS analysis of specimen GC-5 at different ages.

Higher ratios of GFRP powder to GGBS imply that less water is required to dissolve the raw materials. Increasing W/B can improve the flowability of the GGBS geopolymer concrete mixtures while increasing A/B reduces the flowability of the mixture. When S/A was increased from 0.25 to 0.3, the added fine aggregates filled the gaps between coarse aggregates, which was beneficial to the mixture flowability. Further increasing S/A from 0.3 to 0.35 had an insignificant effect on the flowability. Excessive amounts of sand (S/A >0.4) can reduce the mixture workability because the entire surface of the sand and coarse aggregates is too large to be covered by the geopolymer binder [52].

3.3.3 Compressive strength

Figure 18 presents the compressive strength of the geopolymer concretes with different GFRP powder contents, W/B, A/B, and S/A values. The geopolymer concrete with 30 wt% GFRP powder (sample GC-5) presented the highest compressive strength among all of the mixtures at 28 days. This is consistent with the geopolymer paste results. Increasing W/B from 0.45 to 0.5 led to an increase in the compressive strength. The appropriate W/B contributes to the dissolution of aluminosilicate materials and subsequent polycondensation. However, further increasing the W/B value from 0.5 to 0.55 reduced the compressive strength

Table 7: Test results of GFRP powder/GGBS-based geopolymers concretes

Mixture	Initial setting time (min)/δ (%)	Final setting time (min)/δ (%)	Slump (mm)/δ (%)	Compressive strength (MPa)/δ (%)	Elastic modulus (GPa)/δ (%)	Flexural strength (MPa)/δ (%)	RCF
GC-1	164/2.6	189/3.6	170/2.6	50.8/4.1	19.3/1.5	5.7/1.6	8.91
GC-2	196/3.1	258/4.4	211/4.5	34.6/2.5	7.4/1.1	4.6/0.7	7.52
GC-3	205/3.6	265/2.0	242/3.0	23.1/2.5	6.4/1.2	4.0/1.5	5.78
GC-4	166/2.0	195/3.1	185/4.6	49.2/5.1	21.9/0.5	7.2/1.1	6.83
GC-5	175/1.0	211/2.6	201/1.7	58.5/1.5	23.5/1.7	9.7/1.7	6.03
GC-6	220/2.6	243/4.4	230/2.1	52.3/2.7	19.9/1.2	7.7/1.1	6.79
GC-7	188/4.4	230/4.2	212/3.1	50.5/3.9	19.1/0.9	7.6/2.3	6.64
GC-8	178/4.6	225/5.0	198/4.4	56.4/2.2	20.7/0.7	8.2/0.8	6.88
GC-9	182/2.0	232/2.6	215/4.2	46.6/2.4	16.8/0.6	6.4/2.2	7.28
GC-10	179/2.1	224/1.7	205/5.0	49.7/3.8	17.0/1.8	8.5/0.2	5.85

Note: δ is the coefficient of variation.

due to more water and hence higher porosity in the gels. When the A/B value was increased from 4.0 to 5.0, the compressive strength of the geopolymer concrete increased by 26%. The aggregates formed a rigid skeleton of granular elements, which are responsible for the compressive strength. Compared with other parameters, the S/A showed an insignificant effect on the compressive strength. The mixture with S/A = 0.35 presented the highest compressive strength among all of the mixtures.

3.3.4 Flexural strength

The variation trends of the flexural strength of the geopolymer concrete with the four mixture factors are similar to those of the compressive strength. The RCF value of the geopolymer concrete with GGBS alone is 8.91. For identical ratios of W/B, A/B, and S/A, the RCF values of the GGBS geopolymer concrete with 30, 50, and 70 wt% GFRP powder were 6.03, 7.52, and 5.78, respectively. The RCF value of the specimen containing 50 wt% GFRP power was higher than that of the specimen containing 30 wt% GFRP powder. This may be because the resin impregnated on the surface of the glass fiber powder hindered the further dissolution of aluminosilicate materials. When the GFRP powder content was increased from 50 to 70 wt%, the unreacted GFRP powder filled the gaps and hindered the expansion of the harmful pores, leading to a decrease of the RCF value. The incorporation of the GFRP powder can generally improve the brittleness of the GGBS geopolymer concretes. The W/B in the range of 0.45–0.55 and S/A in the range of 0.25–0.35 had an insignificant influence on the RCF values. Increasing the A/B value from 4 to 4.5 led to a reduction of the RCF value from 7.28 to 5.85, whereas further increasing the A/B value had an insignificant effect. The appropriate binder content can therefore effectively improve the compactness of the geopolymer concrete mixture.

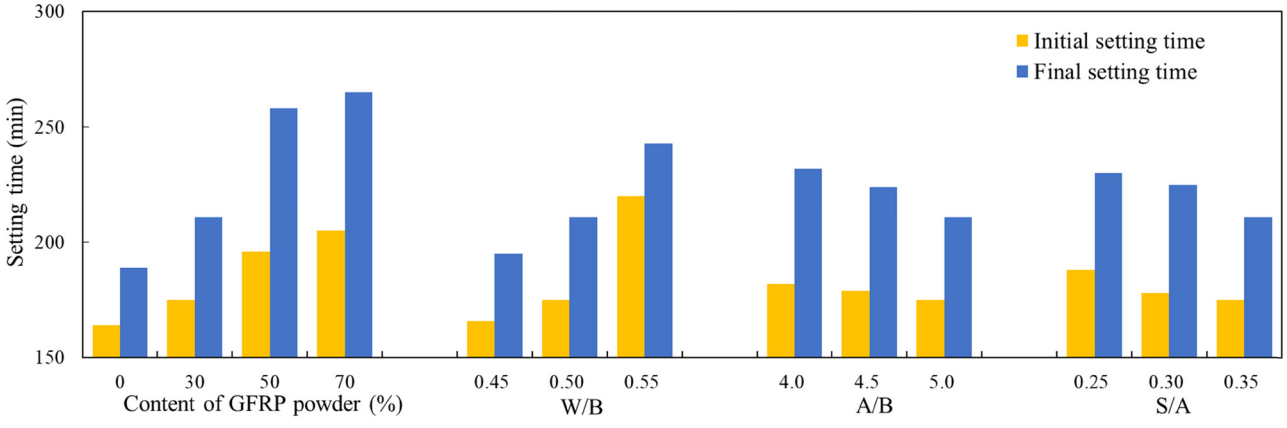

Figure 16: Relationship between the setting time of GFRP powder/GGBS geopolymer concretes and four mix factors.

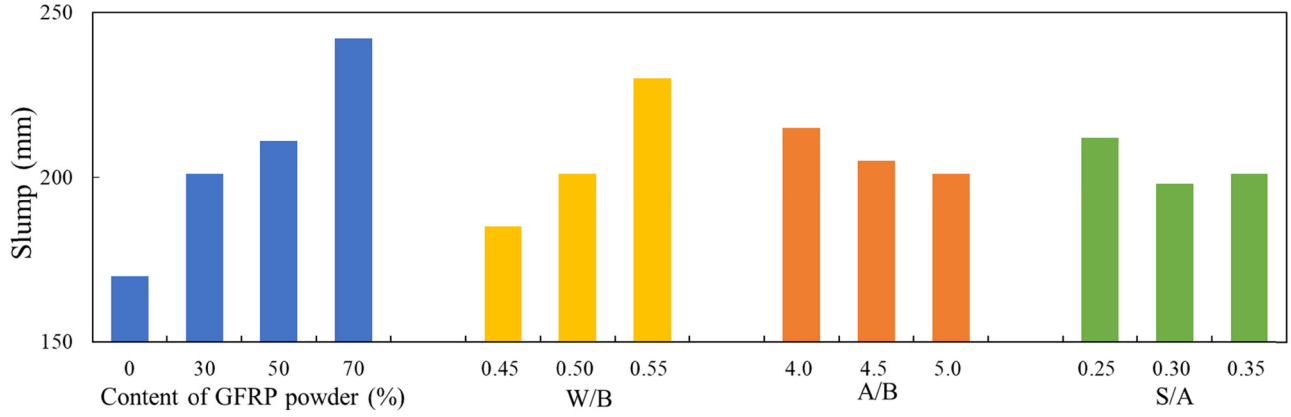

Figure 17: Relationship between the slump of GFRP powder/GGBS geopolymer concretes and four mix factors.

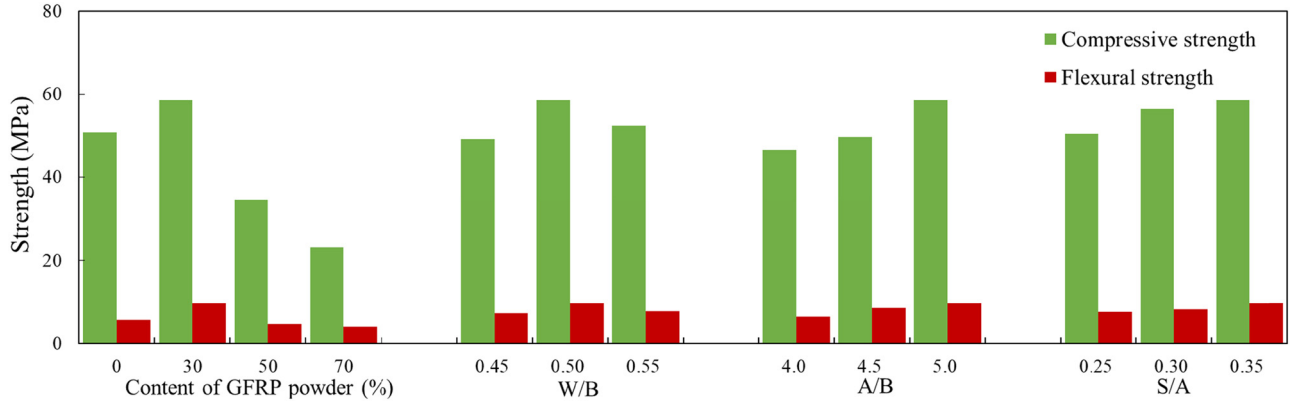

Figure 18: Relationship between the strength of GFRP powder/GGBS geopolymer concretes and four mix factors.

3.3.5 Elastic modulus

The relationship between the elastic modulus of the GFRP powder/GGBS geopolymer concretes and the four mixture factors is shown in Figure 19. The highest elastic modulus is found for the GGBS geopolymer concrete with 30 wt% GFRP powder, which is 22% higher than that of the geopolymer concrete with GGBS alone. This indicates that the

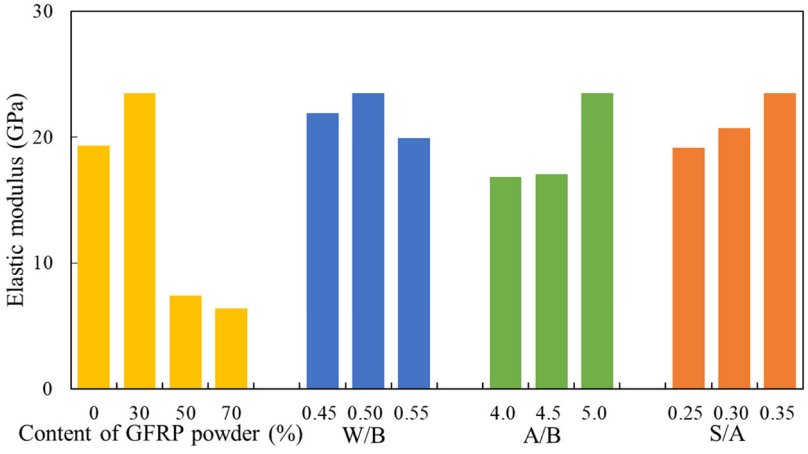

Figure 19: Relationship between the elastic modulus of GFRP powder/GGBS geopolymer concretes and four mix factors.

GGBS geopolymer concrete containing 30 wt% GFRP powder has a better load-bearing skeleton and higher deformation resistance than the geopolymer concrete of GGBS alone. For a given GFRP powder content, A/B, and S/A, the highest elastic modulus was found in the specimen with a W/B value of 0.5. Lower W/B values usually produce stronger geopolymer concrete [53]. However, smaller amounts of water may lead to the uncontrolled development of plastic and autogenous shrinkage and reduce the stiffness of the geopolymer concrete [54]. The RCF values also increase with increasing A/B and S/A. The amount of geopolymer binder should be sufficient to cover and bind the aggregates to form a stable skeleton of the geopolymer concrete. Higher S/A results in better geopolymer concrete gradation. In general, the GGBS geopolymer concrete mixture with 30 wt% GFRP powder, W/B = 0.5, A/B = 5, and S/A = 0.35 displayed the highest compressive and flexural strengths and was less brittle.

4 Conclusion

This study explored the development and characterization of an alkali-activated GFRP waste powder binder. The workability and mechanical properties of single GFRP powder geopolymer paste and binary GFRP powder/GGBS geopolymer paste and concrete were investigated. The following conclusions are drawn.

1) The initial and final setting times of thr fresh GFRP powder geopolymer paste are in the range of 138–720 and 450–1,560 min, respectively. The flowability of the GFRP powder geopolymer paste is in the range of 214–290 mm. The early activity of the GFRP powder-based geopolymers can be accelerated by the incorporation of GGBS. Both the initial and final setting times of the GFRP powder/GGBS-based geopolymer pastes were shorter than those of the geopolymer pastes with GFRP powder alone. The flow value gradually increased with increasing GFRP powder content. All of the designed GFRP powder/GGBS geopolymer concrete mixtures are high-flow concretes.
2) The compressive strength of the GFRP powder-based geopolymer paste gradually increases with the curing age. The RCF values of the GFRP powder based-geopolymer paste at 28 days are lower than those of FA-SS-GGBS geopolymers, thus indicating that the brittleness of the geopolymers is improved by the resin in the GFRP powder. The 28-day strength test results indicate an optimal parameter combination for the GFRP powder-based geopolymer of L/S = 0.8, activator concentration = 85%, and activator solution modulus = 1.3. The compressive strength of the GFRP powder/GGBS geopolymer pastes was remarkably enhanced compared with that of the geopolymer pastes with GFRP powder alone. The GGBS geopolymer pastes and concretes containing 30 wt% GFRP powder showed the highest compressive and flexural strengths at 28 days. In general, the GGBS geopolymer concrete mixture with 30 wt% GFRP powder, W/B = 0.5, A/B = 5, and S/A = 0.35 displayed the highest compressive and flexural strengths and was less brittle.
3) Microstructural analysis indicates that layered gels formed in the GFRP powder-based geopolymers at 7 days, whereas a considerable amount of cluster gels was observed on the GFRP powder/GGBS-based geopolymers at all ages. The Ca/Si ratio at 28 days was considerably lower than those at early ages, indicating the formation of either C–S–H gel or C–A–S–H gel in both the GFRP powder-based geopolymers and binary GFRP powder/GGBS-based geopolymers. The presence of a considerable quantity of Na in the gel products of the GFRP powder-based geopolymers at 7 and 28 days indicates the formulation of N–A–S–H in the GFRP powder-based geopolymers. The incorporation of GGBS in the GFRP powder geopolymers led to a reasonable Al/Si atomic ratio for mechanical strength development.

Acknowledgments: This study was financially supported by the National Natural Science Foundation of China (Grant 51578283), Top Six Talent Projects in Jiangsu Province, China (Grant No. JZ-024), and Science and Technology Projects in Jiangsu Construction System, China (Grant 2021ZD05).

Funding information: This study was financially supported by the National Natural Science Foundation of China (Grant 51578283), Top Six Talent Projects in Jiangsu Province, China (Grant No. JZ-024), and Science and Technology Projects in Jiangsu Construction System, China (Grant 2021ZD05).

Author contributions: Chuji Zheng: formal analysis, validation, writing – original draft. Jun Wang: investigation, conceptualization, formal analysis, resources, project administration. Hengjuan Liu: formal analysis, validation. Hota GangaRao: writing – review & editing, methodology. Ruifeng Liang: formal analysis.

Conflict of interest: No potential conflict of interest was reported by the authors.

References

[1] Morales, C. N., G. Claure, A. R. Emparanza, and A. Nanni. Durability of GFRP reinforcing bars in seawater concrete. *Construction and Building Materials*, Vol. 270, 2021, id. 121492.

[2] Bosbach, B., M. Baytekin-Gerngross, E. Sprecher, J. Wegner, M. D. Gerngross, J. Carstensen, et al. Maximizing bearing fatigue lifetime and CAI capability of fibre metal laminates by nanoscale sculptured Al plies. *Composites Part A: Applied Science and Manufacturing*, Vol. 117, 2019, pp. 144–155.

[3] Guo, Z., Q. Zhu, W. Wu, and Y. Y. Chen. Research on bond–slip performance between pultruded glass fiber-reinforced polymer tube and nano-$CaCO_3$ concrete. *Nanotechnology Reviews*, Vol. 9, No. 1, 2020, pp. 637–649.

[4] Chen, J., J. Wang, and A. Ni. Recycling and reuse of composite materials for wind turbine blades: An overview. *Journal of Reinforced Plastics & Composites*, Vol. 38, No. 12, 2019, pp. 567–577.

[5] Rani, M., P. Choudhary, V. Krishnan, and S. Zafar. A review on recycling and reuse methods for carbon fiber/glass fiber composites waste from wind turbine blades. *Composites: Part B, Engineering*, Vol. 215, 2021, id. 108768.

[6] Formela, K., A. Hejna, L. Zedler, X. Colom, and J. Canavate. Microwave treatment in waste rubber recycling – recent advances and limitations. *Express Polymer Letters*, Vol. 13, No. 6, 2019, pp. 565–588.

[7] Caballero, B. M., I. de Marco, A. Adrados, A. Lpez-Urionabarrenechea, J. Solar, and N. Gastelu. Possibilities and limits of pyrolysis for recycling plastic rich waste streams rejected from phones recycling plants. *Waste Management*, Vol. 57, No. 1, 2016, pp. 226–234.

[8] Davidovits, J. *Geopolymer Chemistry and Applications*, Geopolymer Institute, Saint-Quentin, France, 2008.

[9] Lingyu, T., H. Dongpo, Z. Jianing, and W. Hongguang. Durability of geopolymers and geopolymer concretes: A review. *Reviews on Advanced Materials Science*, Vol. 60, No. 1, 2021, pp. 1–14.

[10] Hasnaoui, A., E. Ghorbel, and G. Wardeh. Effect of curing conditions on the performance of geopolymer concrete based on granulated blast furnace slag and Metakaolin. *Journal of Materials in Civil Engineering*, Vol. 33, No. 3, 2021, pp. 1–10.

[11] Hosseini, S., N. A. Brake, M. Nikookar, Z. Gnaydin-Sen, and H. A. Snyder. Mechanochemically activated bottom ash-fly ash geopolymer. *Cement & Concrete Composites*, Vol. 118, 2021, id. 103976.

[12] Aziz, A., O. Stocker, I. El Amrani El Hassani, A. P. Laborier, E. Jacotot, A. El Khadiri, et al. Effect of blast-furnace slag on physicochemical properties of pozzolan-based geopolymers. *Materials Chemistry and Physics*, Vol. 258, 2021, id. 123880.

[13] Peng, Z., H. Xu, Z. Yuanxun, W. Jinyi, and H. David. Effect of PVA fiber on mechanical properties of fly ash-based geopolymer concrete. *Reviews on Advanced Materials Science*, Vol. 60, No.1, 2021, pp. 418–437.

[14] Al-Majidi, M. H., A. Lampropoulos, A. Cundy, and S. Meikle. Development of geopolymer mortar under ambient temperature for in situ applications. *Construction and Building Materials*, Vol. 120, 2016, pp. 198–211.

[15] Farinha, C. B., J. de Brito, and R. Veiga. Assessment of glass fibre reinforced polymer waste reuse as filler in mortars. *Journal of Cleaner Production*, 2019, Vol. 210, pp. 1579–1594.

[16] Toniolo, N. and A. R. Boccaccini. Fly ash-based geopolymers containing added silicate waste. A review. *Ceramics International*, Vol. 43, No. 17, 2017, pp. 14545–14551.

[17] Torres-Carrasco, M. and F. Puertas. Waste glass in the geopolymer preparation. Mechanical and microstructural characterisation. *Journal of Cleaner Production*, Vol. 90, 2015, pp. 397–408.

[18] He, P., B. Zhang, J.-X. Lu, and C. S. Poon. A ternary optimization of alkali-activated cement mortars incorporating glass powder, slag and calcium aluminate cement. *Construction & Building Materials*, Vol. 107240, 2020, id. 117983.

[19] Burciaga-Diaz, O., M. Duron-Sifuentes, J. A. Diaz-Guillen, and J. I. Escalante-Garcia. Effect of waste glass incorporation on the properties of geopolymers formulated with low purity metakaolin. *Cement & Concrete Composites*, Vol. 107, 2020, id. 103492.

[20] Shoaei, P., F. Ameri, H. Reza Musaeei, T. Ghasemi, and C. B. Cheah. Glass powder as a partial precursor in Portland cement and alkali-activated slag mortar: A comprehensive comparative study. *Construction & Building Materials*, Vol. 251, 2020, id. 118991.

[21] Tho-In, T., V. Sata, K. Boonserm, and P. Chindaprasirt. Compressive strength and microstructure analysis of geopolymer paste using waste glass powder and fly ash. *Journal of Cleaner Production*, Vol. 172, 2018, pp. 2892–2898.

[22] Rashidian-Dezfouli, H. and P. R. Rangaraju. Comparison of strength and durability characteristics of a geopolymer produced from fly ash, ground glass fiber and glass powder. *Materiales de Construcción*, Vol. 67, No. 328, 2017, pp. 1–13.

[23] Rashidian-Dezfouli, H. and P. Rao. A comparative study on the durability of geopolymers produced with ground glass fiber, fly ash, and glass-powder in sodium sulfate solution. *Construction and Building Materials*, Vol. 153, 2017, pp. 996–1009.

[24] 0623-2824-MTDC. A guide to fiber-reinforced polymer trail bridges (fs.fed.us).

[25] Tabatabaeian, M., A. Khaloo, and H. Khaloo. An innovative high performance pervious concrete with polyester and epoxy resins. *Construction & Building Materials*, Vol. 228, 2019, id. 116820.

[26] Saludung, A., T. Azeyanagi, Y. Ogawa, and K. Kawai. Alkali leaching and mechanical performance of epoxy resin-reinforced geopolymer composite. *Materials Letters*, Vol. 304, 2021, id. 130663.

[27] Zhang, A. Effect of epoxy resin on mechanical properties of metakaolin based geopolymer and microscopic analysis. *Journal of Wuhan University of Technology-Materials Science Edition*, Vol. 35, No. 2, 2020, pp. 431–434.

[28] GB/T 1346-2011. *Test method for water requirement of normal consistency, setting time and soundness of the Portland cement*, National Standards of People's Republic of China, China, 2011.

[29] GB/T 8077-2012. *Method for testing uniformity of concrete admixture*, National Standards of People's Republic of China, China, 2012.

[30] GB/T 50080-2016. *Standard for test method of performance on ordinary fresh concrete*, National Standards of People's Republic of China, China, 2016.
[31] GB/T 17671-1999. *Method of testing cements-determination of strength*, National Standards of People's Republic of China, China, 1999.
[32] GB/T50081-2019. *Standard for test methods of concrete physical and mechanical properties*, National Standards of People's Republic of China, China, 2019.
[33] Song, W., Z. Zhu, Y. Peng, Y. Wan, X. Xu, S. Pu, et al. Effect of steel slag on fresh, hardened and microstructural properties of high-calcium fly ash based geopolymers at standard curing condition. *Construction & Building Materials*, Vol. 229, 2019, id. 116933.
[34] Elyamany, H. E., A. E. M. Abd, and A. M. Elmoaty. Setting time and 7-day strength of geopolymer mortar with various binders. *Construction & Building Materials*, Vol. 187, 2018, pp. 974–983.
[35] GB/T 175-2007. *Common portland cement*, National Standards of People's Republic of China, China, 2007.
[36] Chindaprasirt, P., P. De Silva, K. Sagoe-Crentsil, and S. Hanjitsuwan. Effect of SiO_2 and Al_2O_3 on the setting and hardening of high calcium fly ash-based geopolymer systems. *Journal of Materials Science*, Vol. 47, No. 12, 2012, pp. 4876–4883.
[37] Rattanasak, U., K. Pankhet, and P. Chindaprasirt. Effect of chemical admixtures on properties of high-calcium fly ash geopolymer. *International Journal of Minerals, Metallurgy and Materials*, Vol. 18, No. 3, 2011, pp. 364–369.
[38] Temuujin, J., R. P. Williams, and A. van Riessen. Effect of mechanical activation of fly ash on the properties of geopolymer cured at ambient temperature. *Journal of Materials Processing Technology*, Vol. 209, No. 12–13, 2009, pp. 5276–5280.
[39] Huseien, G. F., M. M. Tahir, J. Mirza, M. Ismail, K. W. Shah, and M. A. Asaad. Effects of POFA replaced with FA on durability properties of GBFS included alkali activated mortars. *Construction and Building Materials*, Vol. 175, 2018, pp. 174–186.
[40] Kumar, R. and S. Kumar. Mechanical activation of fly ash: Effect on reaction, structure and properties of resulting geopolymer. *Ceramics International*, Vol. 2, 2011, pp. 533–541.
[41] Erfanimanesh, A. and M. K. Sharbatdar. Mechanical and microstructural characteristics of geopolymer paste, mortar, and concrete containing local zeolite and slag activated by sodium carbonate. *Journal of Building Engineering*, Vol. 32, 2020, id. 101781.
[42] Mahmoodi, O., H. Siad, M. Lachemi, S. Dadsetan, and M. Sahmaran. Development and characterization of binary recycled ceramic tile and brick wastes-based geopolymers at ambient and high temperatures. *Construction and Building Materials*, Vol. 301, 2021, id. 124138.
[43] Guo, X. and X. Pan. Effects of steel slag on mechanical properties and mechanism of fly ash-based geopolymer. *Journal of Materials in Civil Engineering*, Vol. 32, No. 2, 2020, id. 04019348.
[44] Jiang, X., R. Xiao, Y. Ma, M. Zhang, Y. Bai, and B. Huang. Influence of waste glass powder on the physico-mechanical properties and microstructures of fly ash-based geopolymer paste after exposure to high temperatures. *Construction & Building Materials*, Vol. 262, 2020, id. 120579.
[45] Sasui, S., G. Kim, J. Nam, T. Koyama, and S. Chansomsak. Strength and microstructure of class-c fly ash and GGBS blend geopolymer activated in NaOH & NaOH + Na_2SiO_3. *Materials*, Vol. 13, No. 1, 2020, id. 59.
[46] Wang, S., X. Ma, L. He, Z. Zhang, L. Li, and Y. Li. High strength inorganic-organic polymer composites (IOPC) manufactured by mold pressing of geopolymers. *Construction and Building Materials*, Vol. 198, 2019, pp. 501–511.
[47] Singh, B., M. R. Rahman, R. Paswan, and S. K. Bhattacharyya. Effect of activator concentration on the strength, ITZ and drying shrinkage of fly ash/slag geopolymer concrete. *Construction and Building Materials*, Vol. 118, 2016, pp. 171–179.
[48] Ismail, I., S. Bernal, J. Provis, R. Nicolas, S. Hamdan, and J. van Deventer. Modification of phase evolution in alkali-activated blast furnace slag by the incorporation of fly ash. *Cement & Concrete Composites*, Vol. 45, 2014, pp. 125–135.
[49] Xie, T., P. Visintin, X. Zhao, and R. Gravina. Mix design and mechanical properties of geopolymer and alkali activated concrete: Review of the state-of-the-art and the development of a new unified approach. *Construction & Building Materials*, Vol. 256, 2020, id. 119380.
[50] Ren, X. and M. A. Lianyang Zhang. Experimental study of geopolymer concrete produced from waste concrete. *Journal of Materials in Civil Engineering*, Vol. 31, No. 7, 2019, id. 04019114.
[51] GB 50164-2011. *Standard for Quality Control of Concrete*, National Standards of People's Republic of China, China, 2011.
[52] Zhang, J., Y. Ma, J. Zheng, J. Hu, J. Fu, Z. Zhang, et al. Chloride diffusion in alkali-activated fly ash/slag concretes: Role of slag content, water/binder ratio, alkali content and sand-aggregate ratio. *Construction & Building Materials*, Vol. 261, 2020, id. 119940.
[53] Patankar, S. V., S. S. Jamkar, and Y. M. Ghugal. Effect of water-to-geopolymer binder ratio on the production of fly ash based geopolymer concrete. *International Journal of Advanced Technology in Civil Engineering*, Vol. 2, No. 1, pp. 79–83.
[54] Hewlett, P. C. and M. Liska. *Lea's Chemistry of Cement and Concrete*, Butterworth-Heinemann, Oxford, UK, 2019.